Heat Transfer—Japanese Research, 21(6),1992

Heat and Mass Transfer Analysis of Developing Turbulent Flow in a Square Duct

Hitoshi Sugiyama and Mitsunobu Akiyama
Department of Mechanical Systems Engineering
Utsunomiya University
Katsuhiro Shibata
Fuji Heavy Industries, Ltd.

A numerical analysis has been performed on three-dimensional developing turbulent flow in a square duct using a modified Reynolds stress model and a transport equation model for the turbulent flux. Special attention was paid to the relation between the model constants and the Reynolds stress distribution and the developing process of the secondary flow of the second kind. Moreover, using a turbulent heat flux model, the mean Nusselt number was precisely predicted.

Key words: Developing turbulent flow, secondary flow, square duct, turbulent heat flux equation, Reynolds stress model

1. Introduction

Although the configuration of a square duct is simple, it is difficult to predict precisely the Reynolds stress components of turbulent flow in a square duct because turbulent flow in a noncircular duct is accompanied by a secondary flow of the second kind caused by anisotropic turbulence.

The first successful attempt to predict fully developed flow in a square duct was made by Launder and Ying [1] in 1973. On the other hand, a large number of experimental studies have been presented since the experimental work of Nikuradse [2] who was perhaps the first to have observed the secondary motion in noncircular ducts by flow-visualization studies. In recent years, Melling and Whitelaw [3] reported distributions of Reynolds stress components and the secondary flow of the second kind at two cross sections for developing turbulent flow in a square duct by using a laser-Doppler anemometer. However, it seems that an analysis has not been presented of the secondary motion in developing turbulent flow. Although the secondary flow velocity is only of the order of a few percent of the streamwise bulk velocity, the motion influences the friction factor and heat transfer by transporting high-momentum fluid toward the corners. Therefore it is important also industrially to clarify the secondary motion of developing turbulent flow.

The present authors [4] previously reported the advantages and disadvantages of representative Reynolds stress models adopted in many numerical calculations. Concerning these calculated results, the authors [5] modified the pressure-strain term of Reynolds stress equation and examined the validity of the modified Reynolds stress model by comparing the results with the experimental data of Melling and Whitelaw [3] for developing turbulent flow.

ISSN0096–0802/92/0006–0601$7.50/0
©1993 Scripta Technica, Inc.

Table 1

Pressure-Strain Correlations

$\pi_{ij,1} + \pi_{ji,1}$	$-c_1 \frac{\varepsilon}{k}(\overline{u_i u_j} - \frac{2}{3}k\delta_{ij})$
$\pi_{ij,2} + \pi_{ji,2}$	$-\frac{c_2+8}{11}(P_{ij} - \frac{2}{3}P_k\delta_{ij}) + \zeta k\left(\frac{\partial U_i}{\partial x_j} + \frac{\partial U_j}{\partial U_i}\right)$ $-\frac{8c_2-2}{11}(D_{ij} - \frac{2}{3}P_k\delta_{ij})$
$[\pi_{ij} + \pi_{ji}]_w$	$c_1 = c_1^* + c_1' f\left(\frac{L}{X_w}\right),\ c_2 = c_2^* + c_2' f\left(\frac{L}{X_w}\right),\ \zeta = \zeta^* + \zeta' f\left(\frac{L}{X_w}\right)$

In the present study, the first purpose was to clarify the advantages and disadvantages of the modified Reynolds stress model by comparing it to the experimental work by Fujita, Hirota, and Yokosawa [6] who measured the velocity and temperature distributions in fully developed turbulent flow in a square duct. When calculating the temperature field, we adopted a modified transport equation of turbulent heat flux, considering anisotropic turbulence. The second purpose was to examine numerically the behavior of the secondary flow of the second kind and the Reynolds stress components in developing turbulent flow.

2. Nomenclature

a : thermal diffusivity

$C_1, C_2, C_1^*, C_1', C_2^*, C_2', C_{1T}, C_{2T}, C_{1T}^*, C_{2T}^*, C_{2T}'^*, C_{2T}'^*, C_{1T}, w, C_{2T}, w$: empirical constants

D_h : hydraulic diameter

P_k : production of turbulent energy

k : turbulent energy

Re : Reynolds number $= U_b D_h / \nu$

T : time-averaged temperature

T_c : time-averaged central temperature

T_w : time-averaged wall temperature

u : fluctuating velocity

U : time-averaged velocity

U_b : bulk velocity

U_c : central mean flow velocity of cross section

$\alpha, \beta, \eta, \zeta, \upsilon$: empirical constants

Table 2

Constants in Pressure-Strain Correlations

c_1^*	c_2^*	ζ^*	c_1'	c_2'	ζ'
1.4	0.44	-0.16	-0.35	0.12	-0.1

Table 3

Pressure–Temperature Gradient Correlations

$\pi_{iT,1}$	$-c_{1T}\frac{\varepsilon}{k}\overline{u_iT'} - c'_{1T}\frac{\varepsilon}{k}\left(\frac{\overline{u_iu_j}}{k} - \frac{2}{3}\delta_{ij}\right)\overline{u_jT'}$
$\pi_{iT,2}$	$c_{2T}\overline{u_jT'}\frac{\partial U_i}{\partial x_j} - c'_{2T}\overline{u_jT'}\frac{\partial U_j}{\partial x_i}$
$\pi_{iT,w}$	$c_{1T} = c^*_{1T}\left\{1 + c_{1T,w}f\left(\frac{L}{X_w}\right)\right\}$ $c'_{1T} = c'^*_{1T}\left\{1 + c_{1T,w}f\left(\frac{L}{X_w}\right)\right\}$ $c_{2T} = c^*_{2T}\left\{1 + c_{2T,w}f\left(\frac{L}{X_w}\right)\right\}$ $c'_{2T} = c'^*_{2T}\left\{1 + c_{2T,w}f\left(\frac{L}{X_w}\right)\right\}$

ε : turbulent dissipation rate
ν : viscosity constant
π_{ij} : pressure-strain correlating term
π_{iT} : pressure-temperature gradient correlating term
ω : vorticity

3. Turbulent model

3.1 The transport equation of Reynolds stress

A set of differential equations governing the transport of Reynolds stress is derived from the Navier-Stokes equation, namely:

Table 4

Constants in Pressure-Temperature Correlations

$c_{1T}^{\cdot}$	$c_{1T}^{\cdot\cdot}$	$c_{2T}^{\cdot}$	$c_{2T}^{\cdot\cdot}$	$c_{1T,w}$	$c_{2T,w}$
3.9	−2.5	0.8	0.2	0.25	−0.46

$$\frac{D\overline{u_i u_j}}{Dt} = -\overline{u_i u_k}\frac{\partial U_j}{\partial x_k} - \overline{u_j u_k}\frac{\partial U_i}{\partial x_k} + \frac{P_{ij}:\text{production}}{\frac{p}{\rho}\left(\frac{\partial u_i}{\partial x_j} + \frac{\partial u_j}{\partial x_i}\right)}$$

π_{ij} : pressure-strain correlation

$$-\frac{\partial}{\partial x_k}\left\{\overline{u_i u_j u_k} - \nu\frac{\partial \overline{u_i u_j}}{\partial x_k} - \overline{\frac{p}{\rho}(\delta_{jk}u_i + \delta_{ik}u_i)}\right\} \tag{1}$$

Diff_{ij} : diffusion

$$-2\nu\overline{\frac{\partial u_i}{\partial x_k}\frac{\partial u_j}{\partial x_k}}$$

ε_{ij} : dissipation

For the convection and diffusion terms, the approximation proposed by Rodi [7] is used, which performs the calculations by means of an algebraic stress model.

An especially troublesome feature of the Reynolds stress equation is that it is difficult to decide in what way we should express the pressure-strain term shown as the second term of the right-hand side in the above equation. For this pressure-strain term, the authors [5] previously modeled it as shown in Table 1. In Table 1, $\pi_{ij,1}$, $\pi_{ij,2}$, and $\pi_{ij,w}$ are relevant to the interaction of the fluctuating velocities, to that of the mean strain and fluctuating velocities and to the wall effect, respectively.

The constants' values were determined by applying the Reynolds stress equations to homogeneous turbulent shear flow and near-wall turbulence, as shown in Table 2. For homogeneous turbulent flow, the experimental data of Champagne, Harris, and Corrsin [8] (P_k/ε = 1.0) and Harris, Graham, and Corrsin [9] (P_k/ε = 1.55) were used to determine the constants.

3.2 Transport equation of turbulent heat flux

The equations governing the transport of heat flux in turbulent field may be written as follows (when the buoyancy effect and the viscous diffusion term are neglected):

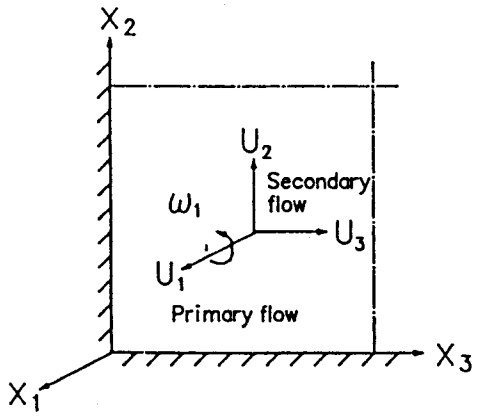

Fig. 1. Calculated region and coordinate system.

$$\frac{D\overline{u_iT'}}{Dt} = -\overline{u_iu_j}\frac{\partial T}{\partial x_i} - \overline{u_jT'}\frac{\partial U_i}{\partial x_j} + \overline{\frac{p}{\rho}\frac{\partial T'}{\partial x_i}}$$

P_{iT} : production π_{iT} : pressure - temperature gradient correlation

$$-\frac{\partial}{\partial x_j}\left(\overline{u_iu_jT'} + \overline{\frac{p}{\rho}T'\delta_{ij}}\right) - (\nu + a)\overline{\frac{\partial T'}{\partial x_j}\frac{\partial u_i}{\partial x_j}} \qquad (2)$$

Diff_{iT} : diffusion ε_{iT} : dissipation

For the convection and diffusion terms, Rodi's proposal [7] was applied to this equation as well as to the Reynolds stress equation. The pressure-temperature gradient correlation is the counterpart of the pressure-strain term in the Reynolds stress equation. In parallel with the pressure-strain term, the pressure-temperature gradient correlation consists of a turbulence interaction part $\pi_{iT,1}$, a mean-strain part $\pi_{iT,2}$ and a wall effect part $\pi_{iT,w}$ as shown in Table 3. The pressure-temperature gradient correlation adopted in this study was that which was proposed by Launder [10]. The values of the constants of the pressure-temperature gradient correlation are shown in Table 4. The fourth term of the right-hand side of Eq. (2) represents the viscous dissipation which will be negligible in local isotropic turbulence at high Reynolds number turbulent flow.

4. Technique of Analysis

4.1 Coordinate system

The object of the analysis is the entrance region of a square duct. As shown in Fig. 1, the calculation domain is taken as one-fourth of the whole cross-section in consideration of symmetry,

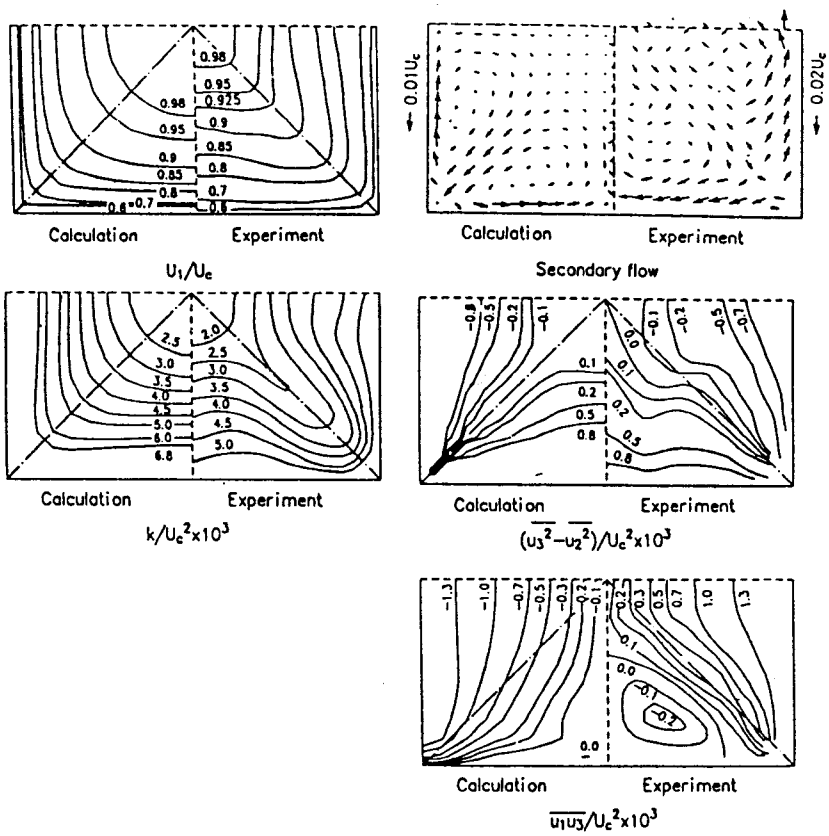

Fig. 2. Comparison of calculated results with experiment.

and X_1 represents the axis of mean flow direction and X_2 and X_3 are the axes of secondary flow direction.

4.2 Calculation object of the analysis

Fujita et al. [11] measured the Reynolds stress components at a cross section $X_1 = 89.8\ D_h$ (total entrance length L = 4,500 mm, side of square duct D = 500 mm) for developing turbulent flow in a square duct by using a hot-wire anemometer. The Reynolds number was set at 65,000.

They also measured time-averaged temperature at a cross section $X_1 = 93.4\ D_h$ corresponding to a location 33 D_h from the point of heating. For the length of 35 D_h from the outlet, wall temperature was set to be constant.

In the present numerical analysis, the entrance length was set at 100 D_h and the calculation grids to be 10 x 10 x 120. The governing equations were transformed to a kind of parabolic equa-

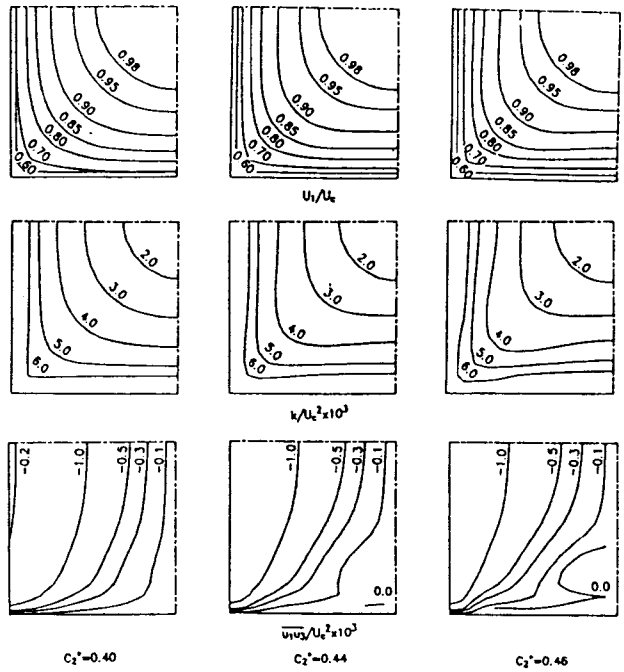

Fig. 3. Contour maps influenced by changing the model constants.

tions by neglecting the streamwise diffusion terms. The turbulent energy and the turbulent dissipation are not specified in the experimental data of Fujita et al. or in the experimental data of Melling and Whitelaw, so that the values of $k = U_b \times 10^5$, $\varepsilon = k^{3/2}/D_h$ were adopted at the inlet section.

5. Results and Considerations

5.1 Analysis of the velocity field

Figure 2 shows a comparison between the experimental and computational results at the cross section at $X_1 = 89.8\, D_h$. The experimental data of mean flow velocity and turbulent energy display a greater bulging of contours caused by the secondary flow of the second kind than the calculated results. For the secondary motion, the present method underestimated its value, compared with the experimental data. And although the measured results of shear stress $\overline{u_1 u_3}$ have both positive and negative values, the calculated results show only negative ones. This discrepancy between the experimental shear stress and the calculated shear stress is caused by the intensity of the secondary motion, which is explained as follows. The equation for the shear stress component $\overline{u_1 u_3}$ is derived from the Reynolds stress equation, assuming that the terms involving the secondary flow velocity are negligible.

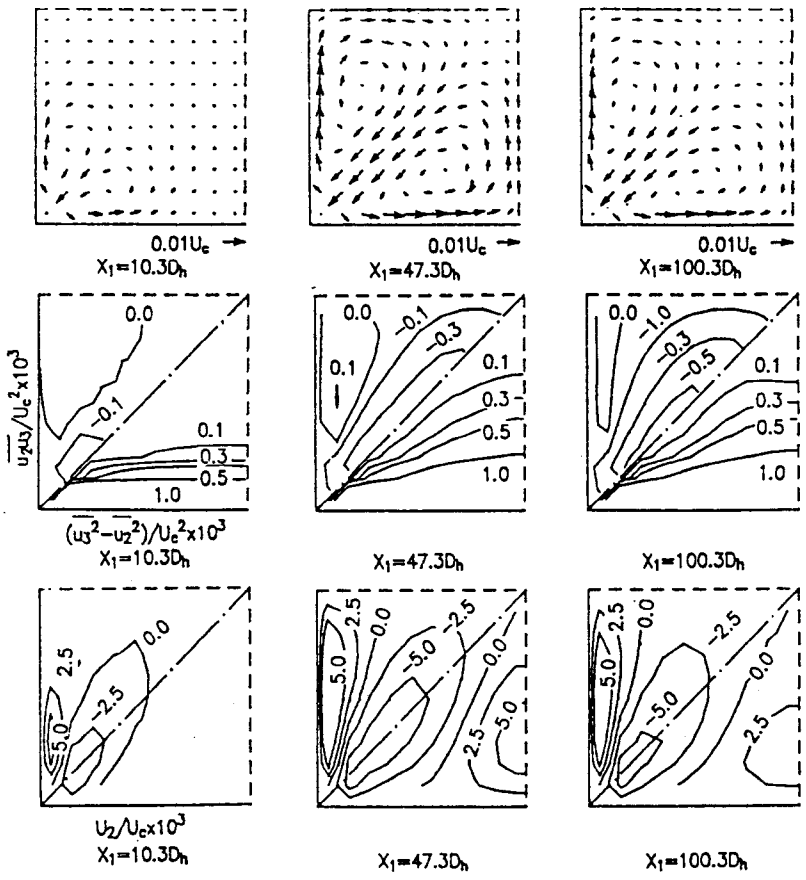

Fig. 4. The development of the secondary flow of the second kind.

$$\overline{u_1 u_3}\left\{\frac{P_k}{\varepsilon}-1+c_1+\frac{k}{\varepsilon}(1+3\beta)\frac{\partial U_1}{\partial x_1}\right\}$$

$$=-\left\{\frac{k}{\varepsilon}(1-\alpha-\beta)\overline{u_3^2}+\frac{k}{3}(4\beta+\alpha)\overline{u_1^2}+\frac{\zeta k^2}{\varepsilon}\right\}\times\frac{\partial U_1}{\partial x_3} \tag{3}$$

The above equation suggests that the positive or negative value of shear stress is governed by the value of velocity gradient $\partial U_1 / \partial x_3$. In other words, distortion of the contours of mean flow velocity toward the corner along the wall bisector and toward the central region along the wall bisector leads to the appearance of the different-sign region of the shear stress.

As shown in Fig. 2, the present Reynolds stress model has a tendency to underestimate the value of the secondary flow of the second kind. This tendency is explained as follows. The generation mechanism of the secondary flow of the second kind is different from that of the secondary

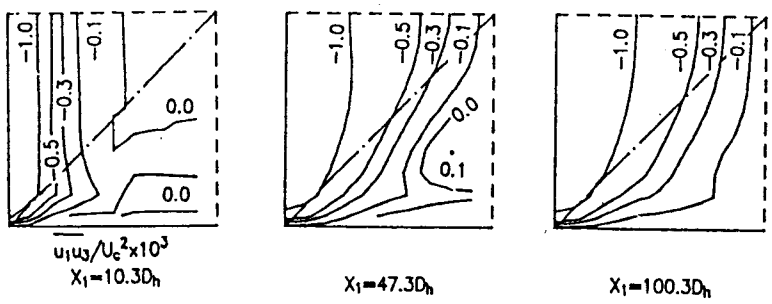

Fig. 5. The development of the shear stress $\overline{u_1u_3}$.

flow in a curved duct where centrifugal forces act at right angle to the main flow direction. The equation for the streamwise vorticity ω_1 for fully developed flow has the following form:

$$U_2\frac{\partial\omega_1}{\partial x_2}+U_3\frac{\partial\omega_1}{\partial x_3}=\nu\left(\frac{\partial^2\omega_1}{\partial x_2^2}+\frac{\partial^2\omega_1}{\partial x_3^2}\right)$$

$$+\frac{\partial^2}{\partial x_2\partial x_3}\left(\overline{u_3^2}-\overline{u_2^2}\right)-\left(\frac{\partial^2}{\partial x_3^2}-\frac{\partial^2}{\partial x_2^2}\right)\overline{u_2u_3} \tag{4}$$

where

$$\omega_1=\frac{\partial U_2}{dx_3}-\frac{\partial U_3}{\partial x_2} \tag{5}$$

From the above equation, the streamwise vorticity ω_1, namely, the secondary motion, may be said to be generated by the normal stress $\overline{u_3^2}-\overline{u_2^2}$ and the shear stress $\overline{u_2u_3}$. The calculated results of the normal stress $\overline{u_3^2}-\overline{u_2^2}$ and shear stress $\overline{u_2u_3}$ are compared with the experimental data in Fig. 2. Moreover, the equations for these stresses are able to be derived from the Reynolds stress equation, assuming that the terms involving the secondary flow velocity are negligible. These equations are as follows:

$$\overline{u_2^2}-\overline{u_3^2}=\frac{4(4c_2-1)k}{11(P_k-\varepsilon+c_1\varepsilon)}\times\left(\overline{u_2u_1}\frac{\partial U_1}{\partial x_2}-\overline{u_3u_1}\frac{\partial U_1}{\partial x_3}\right)\overline{u_2u_3}$$

$$=-\frac{2(4c_2-1)k}{11(P_k-\varepsilon+c_1\varepsilon)}\times\left(\overline{u_2u_1}\frac{\partial U_1}{\partial x_3}+\overline{u_3u_1}\frac{\partial U_1}{\partial x_2}\right) \tag{6}$$

Judging from the above equation, the values of normal stress and shear stress are controlled by the empirical constants c_1 and c_2. When c_1 is fixed and c_2 is changed, for example, secondary motion is not generated when c_2 is equal to 0.25.

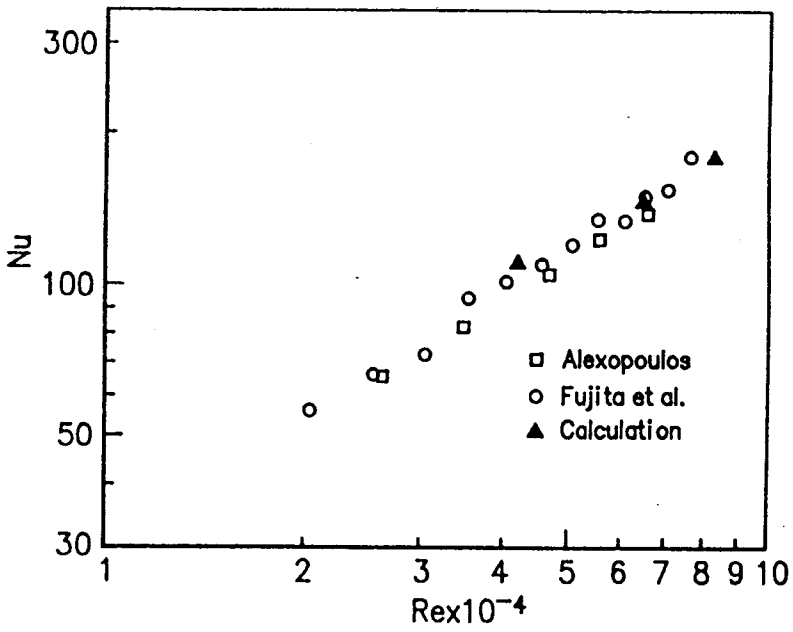

Fig. 6. The relationship between Nusselt and Reynolds number.

In the case where c_2 is changed, the calculated distributions of the mean flow velocity, turbulent energy, and shear stress are shown in Fig. 3. Although c_2 is composed of constants c_2^* and c_2' as shown in Table 2, the calculation was carried out by varying c_2^* only. As the value of the constant becomes larger, the distortion of the counters is shown more clearly. Especially in the distribution of shear stress, both negative and positive sign regions are recognized. From the above consideration, the value of the secondary flow of the second kind may be said to be governed by the constant c_2 which appears in the pressure-strain term. It is a special feature that the generation of the different sign region is shown as a result of a small variation of the constant c_2.

5.2 Developing of the secondary flow of the second kind

There have been many experimental investigations of the secondary flow of the second kind in noncircular ducts since the experimental work of Nikuradse [2]. On the other hand, a large number of numerical investigations have been presented in order to develop the anisotropy turbulent model, since the effective-viscosity formulation cannot predict the secondary flow induced by the turbulent stress field. The first successful attempt to predict the secondary motion in a square duct was made by Launder and Ying [1] in 1973. But there have been few investigations of secondary motion in developing turbulent flow field in a noncircular duct either experimental or numerical. As for one of the reasons for this, it could be pointed out that it is very difficult experimentally to measure the flow field for a long entrance length by a hot-wire anemometer. However, a laser-Doppler anemometer is an effective measuring implement for developing flow, but Melling and Whitelaw, who applied it to a square duct flow, did not present the developing behavior of the

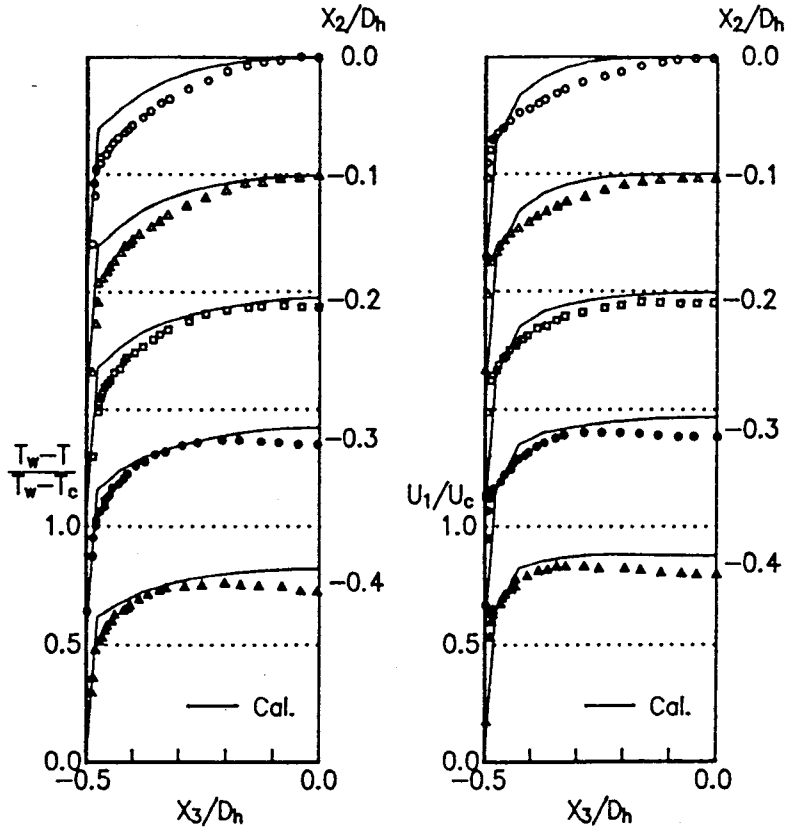

Fig. 7. Comparison of velocity and temperature distributions.

secondary motion. Considering the lack of available published data, the developing motion of the secondary flow of the second kind is examined in this study involving the distribution of normal stress and shear stress.

Figure 4 shows the distributions of secondary flow velocity vector, normal stress, shear stress, and secondary velocity at three locations X_1 = 10.3 D_h, X_2 = 47.3 D_h and X_1 = 100.3 D_h. Generally speaking, the local peaking of the axial center-line velocity occurs as a result of the shear layers' developing from the four walls of the square duct and beginning to merge into one another. The cross section at X_1 = 47.3 D_h corresponds to the location at which this local peaking of the axial center-line velocity is observed. At the cross section X_1 = 10.3 D_h, the secondary flow of the second kind is generated near the corner wall, and the maximum value of the secondary velocity is also observed near the wall of the corner region. Moreover, the distributions of normal stress show large values in the same region. At the cross section X_1 = 47.3 D_h which corresponds to the location of activating momentum transfer, it can be seen that the secondary vector, normal stress, and shear stress largely develop in a quadrant of the duct cross section. The maximum value

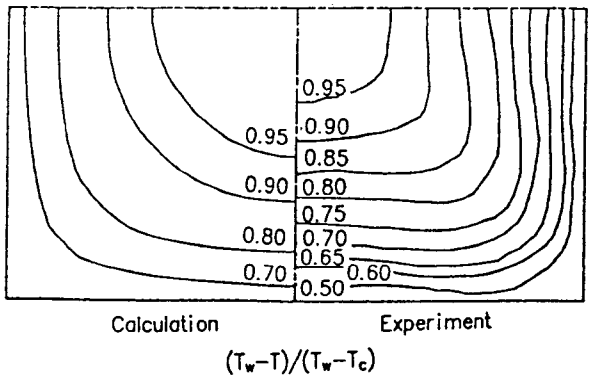

Fig. 8. Comparison of isothermal lines.

of the secondary velocity U_2 is also observed along the corner bisector as well as along the wall. Furthermore, considering the flow developing at the cross section $X_1 = 100.3\ D_h$, the intensity of the secondary motion along the mean flow direction is smaller than that at the cross section $X_1 = 47.3\ D_h$. This decrease of intensity could be explained from the calculated results of the secondary velocity distributions. Judging from these calculated results, the intensity of the secondary flow of the second kind increases to approach a constant value after the local peaking of the secondary motion is observed near the location of activating momentum transfer. This characteristic phenomenon attracts interest because it is similar to the development of the mean flow center-line velocity. Figure 5 shows the distributions of the shear stress $\overline{u_2 u_3}$ in the entrance length. As explained in Sect. 5.1, the appearance of both negative- and positive-value regions of this shear stress is concerned with the bulging of the mean flow velocity contours induced by the secondary motion. In other words, the appearance of the different sign regions is controlled by the intensity of the secondary motion. As shown in Fig. 5, the different sign regions of shear stress are clearly recognized at cross section $X_1 = 47.3\ D_h$. These calculated results also give support to the notion that the secondary motion has its maximum intensity in developing turbulent flow.

From these considerations of the calculated results, the developing behavior of the secondary flow of the second kind can be explained as follows. The secondary flow of the second kind is generated near the corner walls of a square duct and runs from the corner toward the wall bisector along the wall. As a result of this motion, the flow is led along the corner bisector toward the corner and a pair of vortices is generated. While the secondary motion is developing, anisotropic turbulence is generated near the corner walls. Furthermore, the flow developing, intensity of the secondary flow of the second kind approaches a constant value, after the local peaking of the secondary motion is observed near the location of activating momentum transfer.

5.3 Analysis of temperature field

Figure 6 shows the calculated results of relationship between Nusselt number and Reynolds number, compared with the experimental data of Fujita et al. [6] and Alexopoulos. The experimen-

tal data of Alexopoulos are quoted from research work presented by Emery, Neighbors, and Gessner [12]. As shown in Fig. 6, the calculated results of Nusselt number display good agreement with the experimental data.

The calculated results of temperature and velocity distribution are compared with the experimental data at cross section $X_1 = 93.4\ D_h$ as shown in Fig. 7. As for the experimental data, it is pointed out as a characteristic feature that the temperature and the velocity distributions at $X_2 = -0.3\ D_h$ and $-0.4\ D_h$ have a tendency to decrease values near the wall $X_3/D_h = 0.0$. This phenomenon is interpreted as a result of transportation of high-temperature and momentum fluid toward the central region in a square duct by the secondary motion. Underestimating the value of the secondary flow of the second kind, the calculated results do not display a tendency of this kind. The calculated contours of the temperature at cross section $X_1 = 93.4\ D_h$ are compared with the experimental data as shown in Fig. 8. As for the calculated results, the bulging of temperature contours is not so remarkable as for the experimental results.

The present method is not able to predict precisely the near-wall behavior of both the velocity and temperature fields as shown in Fig. 7. From this point of view, it may be said that it is necessary to improve the present turbulent model of the near-wall turbulent model.

6. Conclusion

Numerical calculation has been carried out for developing turbulent flow in a square duct by applying a model of the transport equation of Reynolds stress and turbulent heat flux.

When calculating, Rodi's approximation [7] was adopted to save computational time and to construct a simple program. The calculated results were compared with the experimental data of Fujita et al. [6] who had measured turbulent flow in a square duct including the temperature fields. As a result of this examination, the following conclusions were obtained.

The present turbulent model has a tendency to underestimate the value of the secondary flow of the second kind. This tendency is affected by the value of the constants c_1 and c_2 which appears in the pressure-strain term. By theoretical consideration, the secondary motion may be said not to be generated when the value of c_2 equals 0.25 because of the disappearance of normal stresses $\overline{u_3^2} - \overline{u_2^2}$ and shear stress $\overline{u_2 u_3}$. The secondary motion has a maximum value at the location of the activating momentum transfer as a result of shear layers' developing from the four walls of the square duct and beginning to merge with one another. Furthermore, the developing flow intensity of the secondary flow of the second kind increases and approaches a constant value. This developing behavior of the secondary motion coincides with that of the axial center-line velocity. Additionally, reviewing that the secondary flow velocities have a maximum value near the corner walls from the initial stage of developing, it can be estimated that anisotropic turbulence is produced near the corner walls. The calculated Nusselt numbers show good agreement with the experimental data by using the turbulent heat flux model, but the bulging of the temperature contours is not so distinct as in the experimental data.

It may be said that the present method is effective for the analysis of anisotropic turbulent flow without wasting the computational time. Moreover, we realize the value of the anisotropic

turbulent model only when we apply it to complicated flows. Therefore it is necessary, if applying the anisotropic turbulent model to complicated flows, to modify it to express the near-wall turbulence.

Literature Cited

1. B.E. Launder and W.H. Ying. 1973. *Heat Fluid Flow*, **3** (2), 115–121.
2. J. Nikuradse. 1962. *VDI-Forschungsh.*, 281.
3. A. Melling and J.H. Whitelaw. 1976. *J. Fluid Mech.*, **78**, 289–315.
4. M. Akiyama, H. Kawamura, T. Serizawa, H. Sugiyama, T. Kunugi, and I. Nishiwaki. 1989. **55** (510) B, 351–357.
5. H. Sugiyama, M. Akiyama, and T. Serizawa. 1990. *Trans. JSME*, **56** (531) B, 124–131.
6. H.Fujita, M. Hirota, and H. Yokosawa. 1989. Memo, Facul. Eng., Nagoya Univ., **40** (2), 327–336.
7. W. Rodi. 1976. *Z. Angew. math. Mech.*, **56**, 219–221.
8. F.H. Champagne, V.G. Harris, and S. Corrsin. 1970. *J. Fluid Mech.*, **41**, 81–139.
9. V.G. Harris, A.H. Graham, and S. Corrsin. 1977. *J. Fluid Mech.*, **81**, 657–587.
10. B.E. Launder. 1975. *J. Fluid Mech.*, **67**, 569–581.
11. H. Fujita, H. Yokosawa, and M. Hirota. 1989. Text of the second C.F.D. workshop. Japan Soc. Mech. Eng.
12. A.F. Emery, P.K. Neighbors, and F.B. Gessner. 1980. *Trans. ASME, J. Heat Transf.*, **102**, 51–57.

□♦♦♦□

Originally published in *Trans. JSME*, **57** (535) B, 1991, 1044–1050.

Translated by Hitoshi Sugiyama, Department of Mechanical Systems Engineering, Utsunomiya University, 2753 Ishii-cho, Utsunomiya 321, Japan.